

Effect of Multiple Reflow Cycles and Al₂O₃ Nanoparticles Reinforcement on Performance of SAC305 Lead-Free Solder Alloy

Sanjay Tikale and K. Narayan Prabhu

(Submitted January 14, 2018; in revised form March 20, 2018; published online May 4, 2018)

The effect of Al₂O₃ nanoparticles reinforcement on melting behavior, microstructure evolution at the interface and joint shear strength of 96.5Sn3Ag0.5Cu (SAC305) lead-free solder alloy subjected to multiple reflow cycles was investigated. The reinforced SAC305 solder alloy compositions were prepared by adding Al₂O₃ nanoparticles in different weight fractions (0.05, 0.1, 0.3 and 0.5 wt.%) through mechanical dispersion. Cu/solder/Cu micro-lap-shear solder joint specimens were used to assess the shear strength of the solder joint. Differential scanning calorimetry was used to investigate the melting behavior of SAC305 solder nanocomposites. The solder joint interfacial microstructure was studied using scanning electron microscopy. The results showed that the increase in melting temperature (T_L) and melting temperature range of the SAC305 solder alloy by addition of Al₂O₃ nanoparticles were not significant. In comparison with unreinforced SAC305 solder alloy, the reinforcement of 0.05-0.5 wt.% of Al₂O₃ nanoparticles improved the solder wettability. The addition of nanoparticles in minor quantity effectively suppressed the Cu₆Sn₅ IMC growth, improved the solder joint shear strength and ductility under multiple reflow cycles. However, the improvement in solder properties was less pronounced on increasing the nanoparticle content above 0.1 wt.% of the solder alloy.

Keywords Al₂O₃ nanoparticles, nanocomposite, multiple reflows, SAC305 lead-free solder, shear strength

1. Introduction

Nanocomposite lead-free solders are gaining more attention recently in electronics and packaging industry. Studies have shown that the addition of nanoparticles in solder improve the solder matrix strength, alter the intermetallic compound (IMC) morphology and suppress IMC growth under various thermal conditions. Solder joints essentially provide the mechanical, electrical and thermal continuity in electronic assemblies. The use of lead-free solder alloys is in the mainstream now due to the strict global legislation to ban the use of lead-containing solder alloys (Ref 1). The reliability of solder joint mainly depends on physical properties like yield strength, elastic modulus, shear strength, fatigue and creep behavior of the solder alloy (Ref 2, 3). The physical and thermal properties of solder joint are largely influenced by intermetallic compound (IMC) layer formed at the joint interface. A thin, continuous and uniform IMC layer at the interface provides a good bonding and improves the joint strength. Excessive growth of IMCs may decrease the physical properties of solder joint due to their inherently brittle nature and tendency to generate structural defects (Ref 4-6). Among the various lead-free solders developed, ternary Sn-Ag-Cu (SAC) solders are considered as one of the most promising substitutes. Sn-Ag-Cu

solders show good reliability and mechanical properties. However, they possess higher melting temperature, poor wettability, and coarser grain structure compared to Sn-Pb solders. Higher Sn content and high melting point of SAC solders enhance the dissolution rate and increase the solubility of Cu in molten SAC solders, leading to an increase in the rate of IMC formation (Ref 7, 8). To make lead-free solders as competitive substitutes for Sn-Pb solder, researchers have developed various methods to improve solder properties. Among various approaches, adding appropriate second-phase material into solder alloy was found to be effective in improving solder properties. The main purpose of addition of second-phase material into solder alloy is to improve the solder joint reliability by refining the solder grain structure and suppress the IMC growth under multiple reflows and thermal aging conditions. The addition of extra alloying elements like In, Bi and Ti resulted in the reduction in melting point and changed the wetting behavior of SAC solders. However, the effect of extra element addition in retarding IMC growth was not significant (Ref 9-11). In the view of the improvement in physical properties and cost-effectiveness of the solder alloy, the development of nanocomposite solder alloys is an affordable and viable approach. Nanocomposite SAC solder alloys can be developed by incorporating metallic or ceramic nanoparticles into solder matrix (Ref 12-15).

Several studies by researchers have shown that the nanoparticles addition strengthens the solder matrix by particle dispersion. Dispersed phase obstructs the dislocation movement and pin grain boundaries in the solder matrix during failure which can improve the solder deformation resistance (Ref 16, 17). Nanoparticles also retard the excessive IMC growth by limiting the diffusion of the relevant element at the interface. Various nanoparticles have been investigated to improve the physical and thermal properties of lead-free solder alloys.

Sanjay Tikale and K. Narayan Prabhu, Department of Metallurgical and Materials Engineering, National Institute of Technology Karnataka, Surathkal 575 025, India. Contact e-mail: prabhukn_2002@yahoo.co.in.

Based on their different physical properties, nanoparticles can be broadly categorized into metallic, ceramic, and carbon nanotubes (Ref 18).

Zhong and Gupta (Ref 19) observed an increase in microhardness, 0.2% yield strength and ultimate tensile strength of Sn-0.7Cu solder along with the decrease in Cu₆Sn₅ IMC layer growth by the addition of Al₂O₃ nanoparticles. Chuang et al. (Ref 20) reported a lower coefficient of thermal expansion (CTE) for Sn_{3.5}Ag_{0.7}Cu and Al₂O₃ nanoparticles composite compared to unreinforced solder. An investigation by Tsao et al. (Ref 21) on Sn_{0.5}Ag_{1.0}Cu-Al₂O₃/Cu soldered joints showed the suppression of Cu₆Sn₅ IMC growth at the joint interface with the addition of Al₂O₃ nanoparticles when subjected to multiple reflow cycles. The IMC thickness of composite solder joint was found to be thinner compared to the bare SAC/Cu solder joint. The authors concluded that the adsorption of Al₂O₃ nanoparticles on the Cu₆Sn₅ IMC grains limits the further dissolution of Cu atoms which reduce the grain ripening and retard the scallop-shaped Cu₆Sn₅ IMC growth.

A limited work has been done on the performance of nanocomposite solder joint under multiple reflow cycles. The effect of Al₂O₃ nanoparticles reinforcement on mechanical properties and interfacial IMC growth of solder joint under repeated reflow cycles is largely unexplored. The aim of this study is to investigate the effect of multiple reflow cycles on melting behavior, intermetallic compounds growth at the joint interface and solder joint shear strength of SAC305 solder alloy reinforced with Al₂O₃ nanoparticles. Experiments were performed with varying amount of Al₂O₃ nanoparticles addition in the solder alloy to determine the optimum weight fraction of nanoparticles addition that would maximize the solder properties under multiple reflow cycles.

2. Materials and Methods

2.1 Sample Preparation and Mechanical Testing

96.5Sn-3Ag-0.5Cu (in wt.%) solder alloy paste (Persang Alloy Industries Pvt. Ltd. Gujarat, India) added with RMA (mildly activated rosin, ROL0) flux was used as the matrix alloy. The Al₂O₃ nanoparticles (average particle size 20-30 nm, Sisco Research Laboratories Pvt. Ltd. Mumbai, Maharashtra, India) were used for reinforcement in solder alloy. The SEM and transmission electron microscope (TEM, JEOL JEM-2100) images with x-ray diffraction pattern for Al₂O₃ nanoparticles used in this study are presented in Fig. 1. Four solder systems were synthesized and characterized by mechanically dispersing Al₂O₃ nanoparticles with 0.05, 0.1, 0.3 and 0.5 (in wt.% related to the mass of solder paste), respectively, into the SAC305 solder paste. These solder systems are designated hereafter as, SAC305-*x*Al₂O₃, where *x* represents weight percentage. Experiments were also performed with unreinforced SAC305 solder paste for comparison. The processing procedure of composite solder involved a direct blending of the required amount of solder paste and nanoparticles. The mixture was blended mechanically for at least 30 min to obtain uniform distribution of nanoparticles in the solder paste.

Mechanical properties of the solder joint were investigated through the tensile pull test of solder joint samples. For the shear test, a micro-lap-shear solder joint specimen was

designed. Figure 2 shows the schematic diagram of micro-lap-shear solder joint specimen used in this study. The test samples were pure (99.9% purity) EC grade copper (Cu) substrates. The surface roughness of copper plates was measured by using surface profilometer (Form Talysurf 50). The surface roughness (*R_a* value) of plates was maintained in the range of 0.1-0.3 μm throughout this study. Copper plates were first precleaned with inorganic flux to remove oxide layer followed by cleaning with acetone. A layer of 0.2 mm thick (0.1 g) of solder paste was sandwiched between the two Cu plates. Samples were assembled with a fixture to maintain the rectangular shape of the solder joint with 0.2 mm solder paste layer. The sample with fixture assembly was heated in an infrared IC heater reflow oven (Puhui T-962) using the thermal reflow profile represented in Fig. 3. A heating rate (ramp rate) of 2 °C/s was used to achieve the temperature above 150 °C. Solder paste then soaked for about 180 s to activate the flux before reaching the reflow temperature of 250 °C followed by the reflow for 100 s. Samples were forced-air cooled to the room temperature with the cooling rate of 2 °C/s. Samples were prepared for the assessment of effect of multiple reflow cycles on joint shear strength and interfacial microstructure by subjecting them to 1, 2, 4 and 6 reflow cycles. The shear test was performed using Instron 5967 tensile testing machine (Instron 5967, 30 kN). In this study, the shear test was conducted for the strain rate of $1 \times 10^{-2} \text{ s}^{-1}$ at the room temperature. Average shear strength for the solder joint of each solder alloy composition was determined from stress-strain curves obtained from the test of at least four samples.

2.2 Melting Behavior and Wettability Analysis

The effect of the addition of nanoparticles on onset and melting temperatures as well as melting temperature range of SAC305 solder alloy was investigated by using differential scanning calorimetry (DSC, 404 F1 Pegasus NETZSCH) under N₂ atmosphere. Solder paste sample (unreinforced and reinforced with nanoparticles) weighted 15.5 mg was placed in the aluminum pan with a lid. A hole was made on the lid for the reaction outgas ventilation. The heating rate of 10 °C/min for the temperature range of 30-300 °C was used for thermal analysis. Thermal reactions for all SAC305 solder alloy composites were determined based on endothermic (heating) curves.

The wettability of SAC305 solder alloy with nanoparticles addition was determined with respect to spreading base area. The measured amount (0.1 g) of different nanocomposite SAC305 solder paste was placed on a polished copper cylindrical substrate using solder paste dispenser. The samples were reflowed in reflow oven by using thermal profile shown in Fig. 3. The stereo micrographs of reflowed samples were captured using stereomicroscope (Stemi 2000-C). The spreading behavior of composite solder was analysed and spreading area was calculated by using Axio Vision SE64 Rel. 4.9 software. The average spreading area was calculated from the measurements on four samples for each solder alloy composition.

2.3 Microstructural Characterization

The effects of Al₂O₃ nanoparticle reinforcement and multiple reflow cycles on morphology and growth of solder joint interfacial IMC were studied using scanning electron microscopy (SEM, JEOL JSM 6380LA). Elemental analysis of IMC and other phases in solder microstructure was carried out

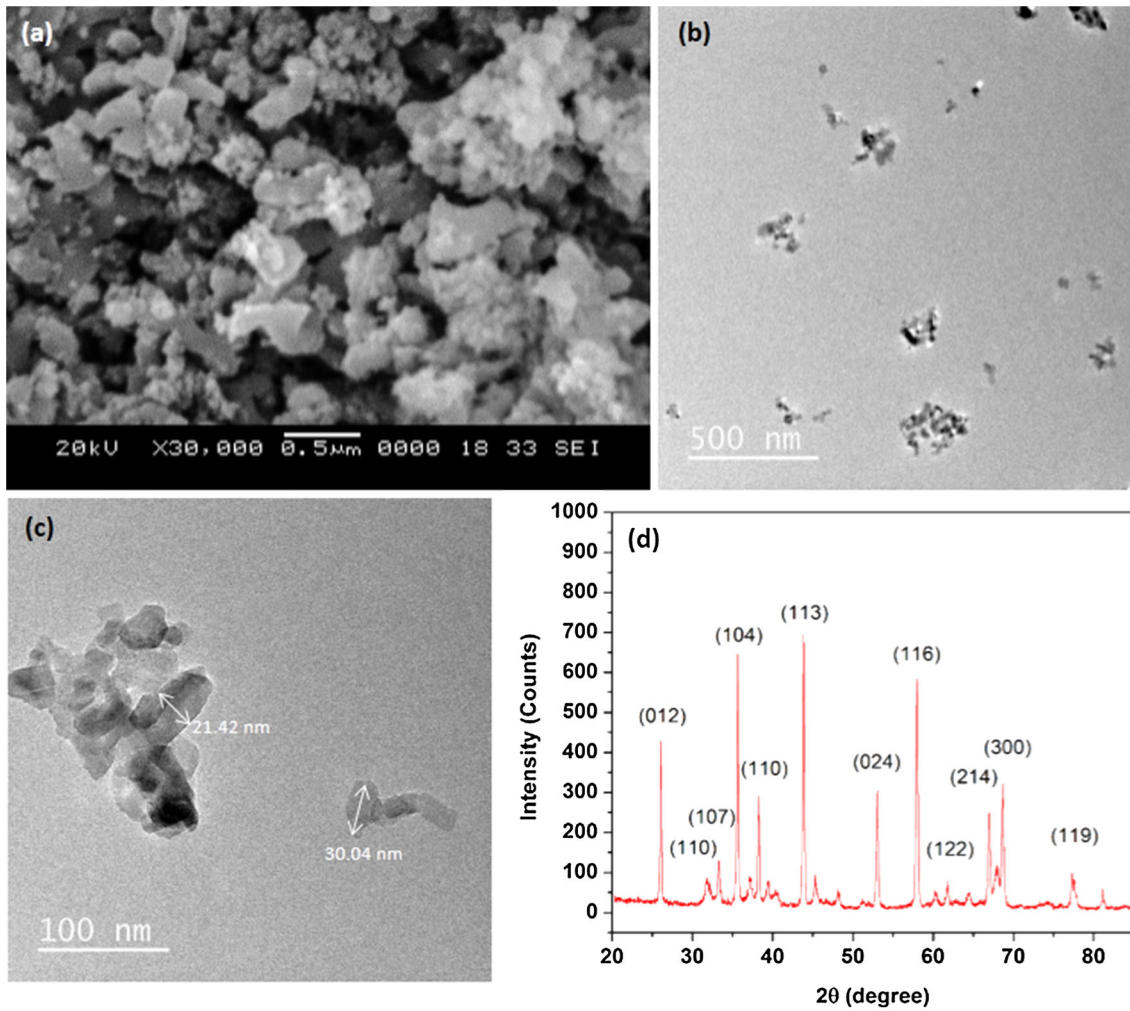


Fig. 1 (a) SEM image of Al₂O₃ nanoparticles, (b) TEM image of dispersed Al₂O₃ nanoparticles, (c) TEM image showing size of Al₂O₃ nanoparticles, (d) XRD pattern for Al₂O₃ nanoparticles

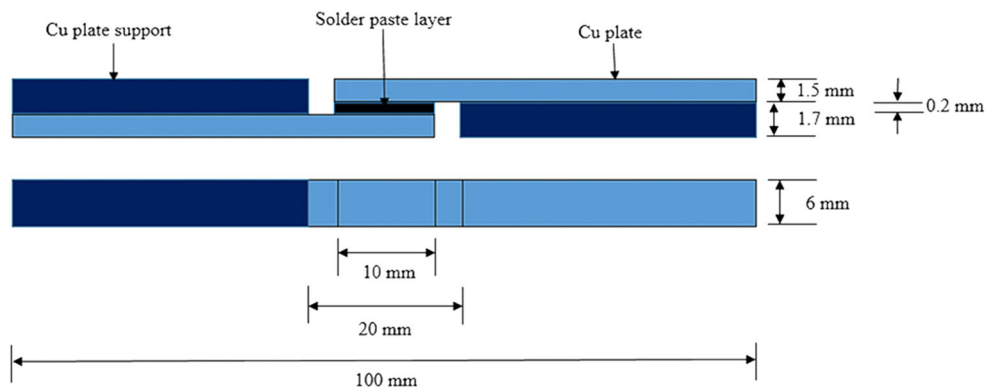


Fig. 2 Schematic diagram of the micro-lap-shear solder joint assembly with copper plate support (front and top view)

using energy-dispersive spectroscopy (EDS). For the study of IMC growth at the solder joint interface, reflowed samples with the nanocomposite SAC305 solder paste were cut and polished with various grit size polishing papers followed by disk polishing with a 0.5-1 μm diamond-lapping compound paste to obtain a highly smooth surface. Polished surfaces were etched with 5% nital solution [Ethanol (C₂H₅OH) and concentrated

nitric acid (HNO₃) in the 95 + 5 volume ratio, respectively.] for 1-2 s. The interfacial IMC thickness was determined by image analysis using Axio Vision SE64 Rel. 4.9 software. IMC thickness was measured in three different regions at the interface for each sample. The IMC layer obtained at the interface was uneven in nature and hence, an average value of IMC thickness (\bar{x}) was determined by using an Eq 1.

$$\bar{x} = A_i/L_x \quad (\text{Eq 1})$$

where A_i is the area and L_x is the length of IMC layer obtained from SEM micrograph represented in Fig. 4.

3. Results and Discussion

3.1 Melting Behavior and Wettability

Heating (endothermic) curve analysis of the composite solder is helpful in understanding the reactions of the solid–liquid transition during soldering. Figure 5 shows the DSC curves for heating cycle of the composite SAC305 solder specimens doped with different wt.% of Al_2O_3 nanoparticles. The onset temperature, melting temperature and melting temperature range of SAC305 solder alloy with different compositions of Al_2O_3 nanoparticles are presented in Table 1. The increase in the onset temperature (T_s) and melting

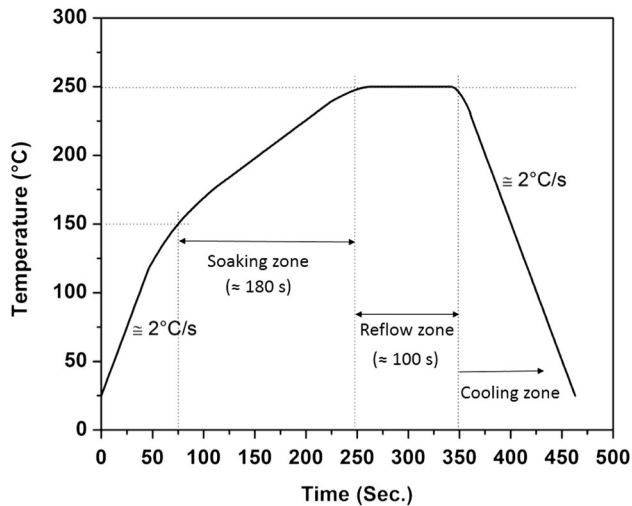


Fig. 3 Reflow temperature profile for Cu/solder/Cu joint preparation

temperature (T_L), as well as the melting range of SAC305 solder alloy with addition of Al_2O_3 nanoparticles was not significant. This suggests that the addition of (0.05-0.5 wt.%) Al_2O_3 nanoparticles will not affect the existing reflow thermal profile and manufacturing setup of PCB production process for SAC305 solder alloy.

Figure 6 shows the spreading area as a function of different wt.% of Al_2O_3 nanoparticles addition in SAC305 solder alloy. The addition of 0.05-0.5 wt.% Al_2O_3 nanoparticles showed an improvement in spreading behavior of SAC305 solder which implies, an enhancement in the wettability of the solder alloy. The work done by Zhong and Gupta (Ref 19) shows that the density of solder alloy decreased with the increasing content of Al_2O_3 nanoparticles. The nanoparticles are highly surface-active and when added to the solder alloy they reduce the surface tension of the liquid solder. The reduction in liquid surface tension also decreases the boundary tension between the liquid solder and solid substrate leading to decrease in contact angle. The enhancement in wettability of the solder alloy after addition of Al_2O_3 nanoparticles is attributed to the decrease in the liquid solder surface tension and interfacial tension between the composite solder and substrate. The increment in spreading area is significant up to 0.3 wt.% Al_2O_3 addition, whereas it is not significant for 0.5 wt.% addition. The investigation on Sn3.5Ag0.5Cu doped with Al_2O_3 nanoparticles also indicated a similar spreading behavior (Ref 21). The addition of Al_2O_3 nanoparticles in minor quantity effectively enhanced the wettability of solder. However, addition of over 0.3 wt.% increases the agglomeration of nanoparticles leading to the reduction of net surface-active material in the liquid solder which diminishes the beneficial effect of nanoparticle addition.

3.2 Solder Joint Microstructure

Sn-Ag-Cu ternary phase diagram is shown in Fig. 7(a). The area indicated in the red box shows the near-eutectic region of SAC solder alloy represented in Fig. 7(b) (Ref 22). The eutectic reaction takes place at the temperature of 217.2 °C. Under equilibrium solidification conditions, the microstructure of near-eutectic SAC solders mostly consists three phases: a high-volume fraction of β -Sn matrix containing small, needle, or disk-shaped particles of Ag_3Sn and Cu_6Sn_5 IMCs. SEM micrographs of SAC305 solder/Cu substrate joint interface

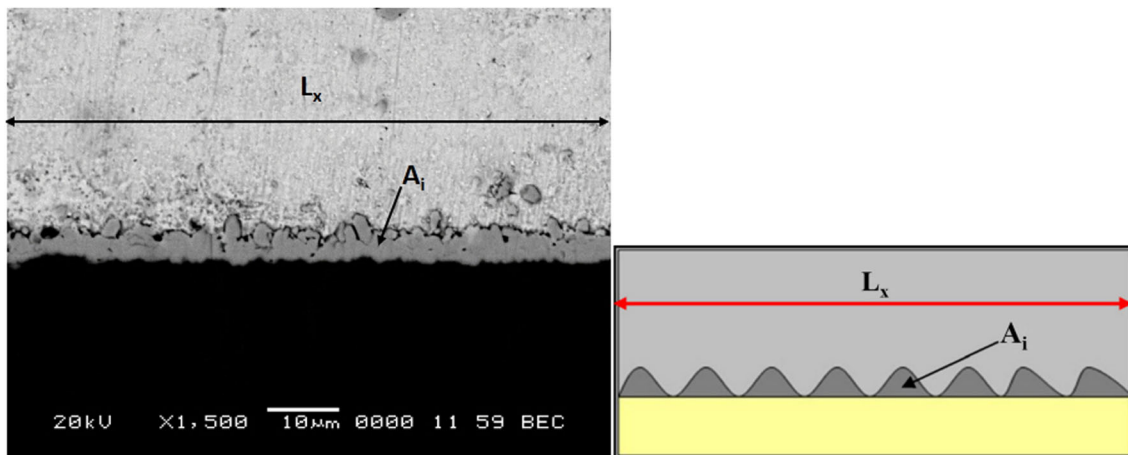


Fig. 4 Representative SEM micrograph showing interfacial IMC layer of the solder joint after reflow

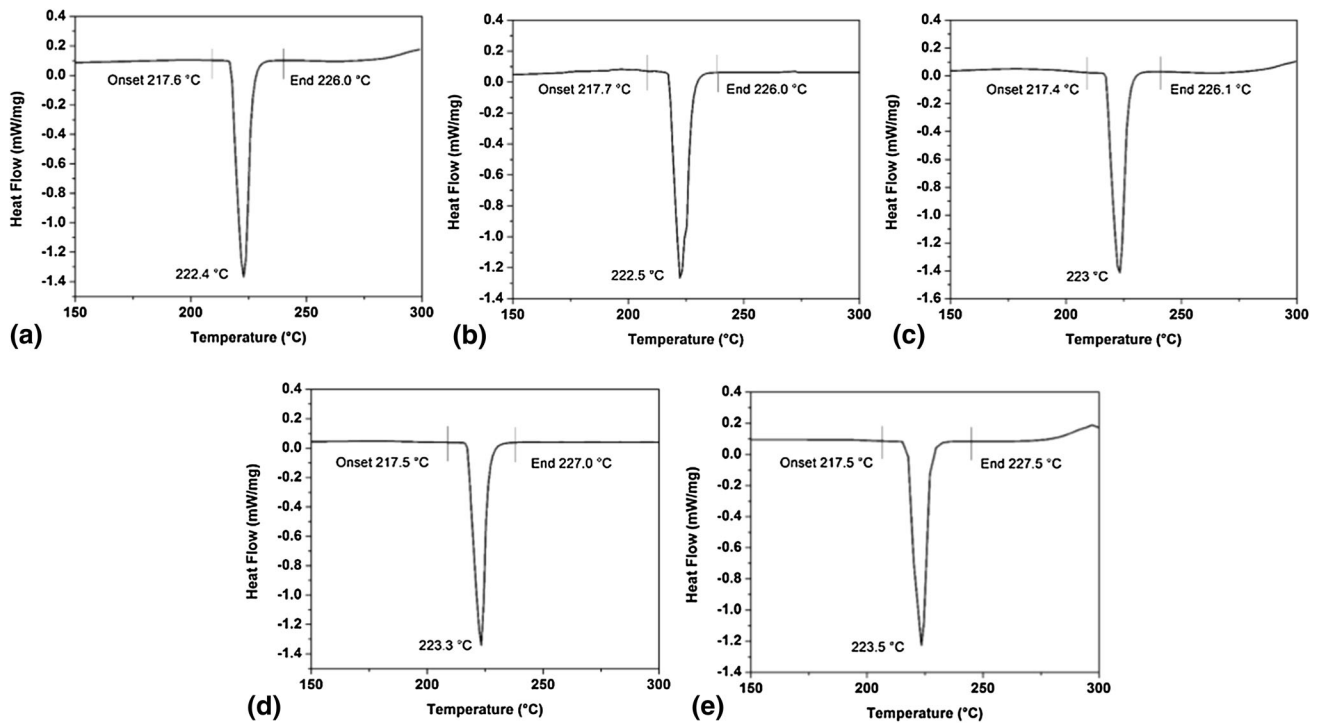


Fig. 5 DSC curves for the heating cycle of SAC305 solder alloy with different wt.% of Al_2O_3 nanoparticles compositions, (a) SAC305, (b) SAC305-0.05 Al_2O_3 , (c) SAC305-0.1 Al_2O_3 , (d) SAC305-0.3 Al_2O_3 , (e) SAC305-0.5 Al_2O_3

Table 1 Onset temperature, melting temperature and melting temperature range of SAC305 solder alloy with different Al_2O_3 nanoparticles compositions

Solder alloy composition	Onset temperature, T_s , °C	Melting temperature, T_L , °C	Melting temperature range, ΔT , °C
SAC305	217.6	222.4	4.8
SAC305-0.05 Al_2O_3	217.7	222.5	4.8
SAC305-0.1 Al_2O_3	217.4	223.0	5.6
SAC305-0.3 Al_2O_3	217.5	223.3	5.8
SAC305-0.5 Al_2O_3	217.5	223.5	6.0

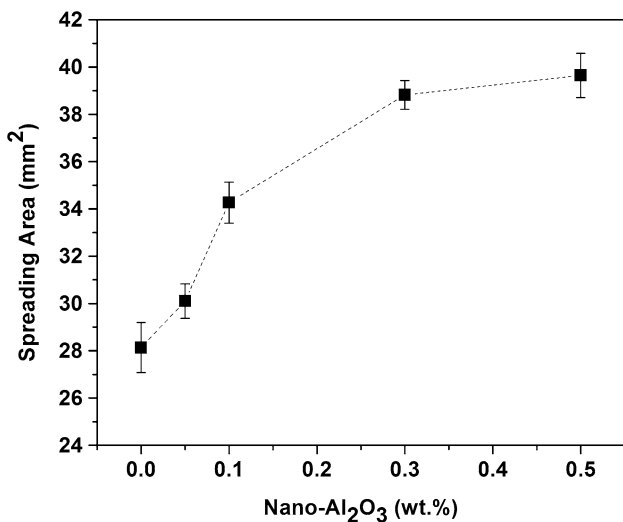


Fig. 6 Spreading area as a function of weight fraction of Al_2O_3 nanoparticles addition

with and without the addition of Al_2O_3 nanoparticles for multiple reflow cycles are presented in Fig. 8. With the help of EDS analysis, the Cu_6Sn_5 IMC was confirmed as major IMC formed at the interface and Ag_3Sn IMC formed in the bulk solder. The observed Cu_6Sn_5 and Ag_3Sn IMCs are shown in SEM micrographs presented in Fig. 8. The EDS graphs showing peaks for different IMCs with the percentage of elemental composition is presented in Fig. 9. The morphology and growth of Cu_6Sn_5 IMC changed with respect to the amount of nanoparticles addition and reflow cycles. The morphology of Cu_6Sn_5 IMC appeared scallop shaped for unreinforced SAC305 solder alloy and with increase in reflow cycles, the IMC become thicker and elongated. The Ag_3Sn IMC morphology transformed from coarser to finer spheroidal shape with increase in reflow cycles. After four reflow cycles, the formation of thin and discontinuous Cu_3Sn IMC layer was observed between Cu substrate and Cu_6Sn_5 IMC layer. The x-ray diffraction (XRD) plot for unreinforced SAC305 solder sample taken at the solder joint interface is shown in Fig. 10. The figure shows the peaks for all IMCs present in the

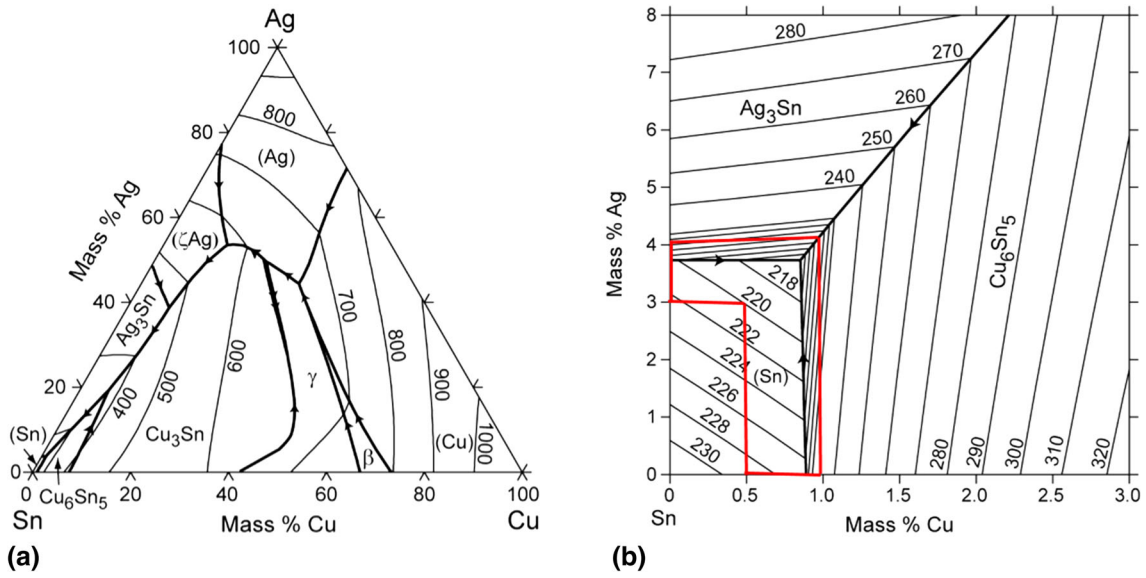


Fig. 7 Phase diagram: (a) Sn-Ag-Cu ternary phase diagram, (b) phase diagram showing near-eutectic region for SAC solder alloy (Ref 22)

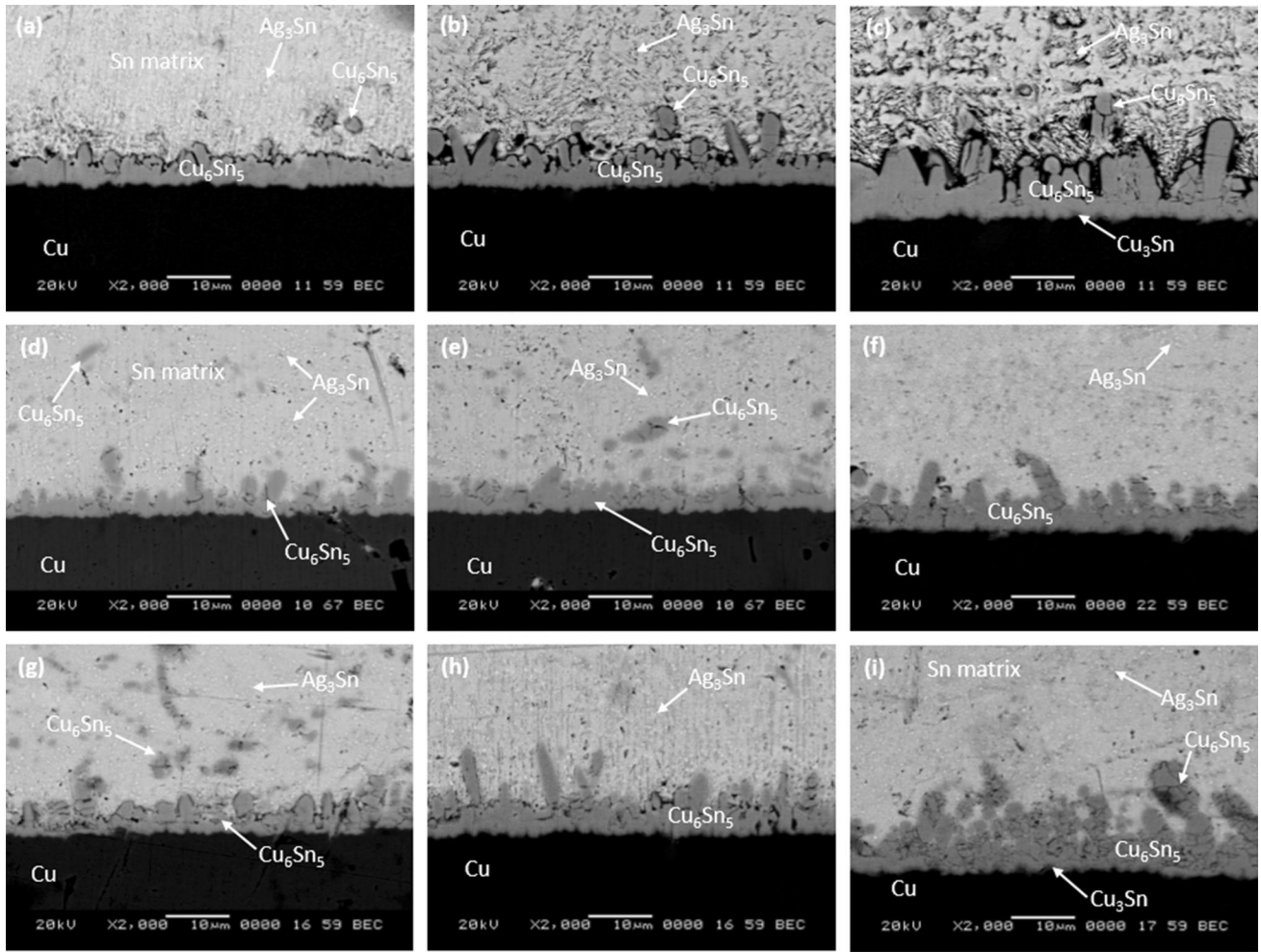


Fig. 8 SEM micrographs of solder/Cu substrate joint interface for multiple reflow cycles: (a) one reflow, (b) two reflow, (c) six reflow for unreinforced SAC305; (d) one reflow, (e) two reflow, (f) six reflow for SAC305-0.1Al₂O₃; (g) one reflow, (h) two reflow, (i) six reflow for SAC305-0.5Al₂O₃

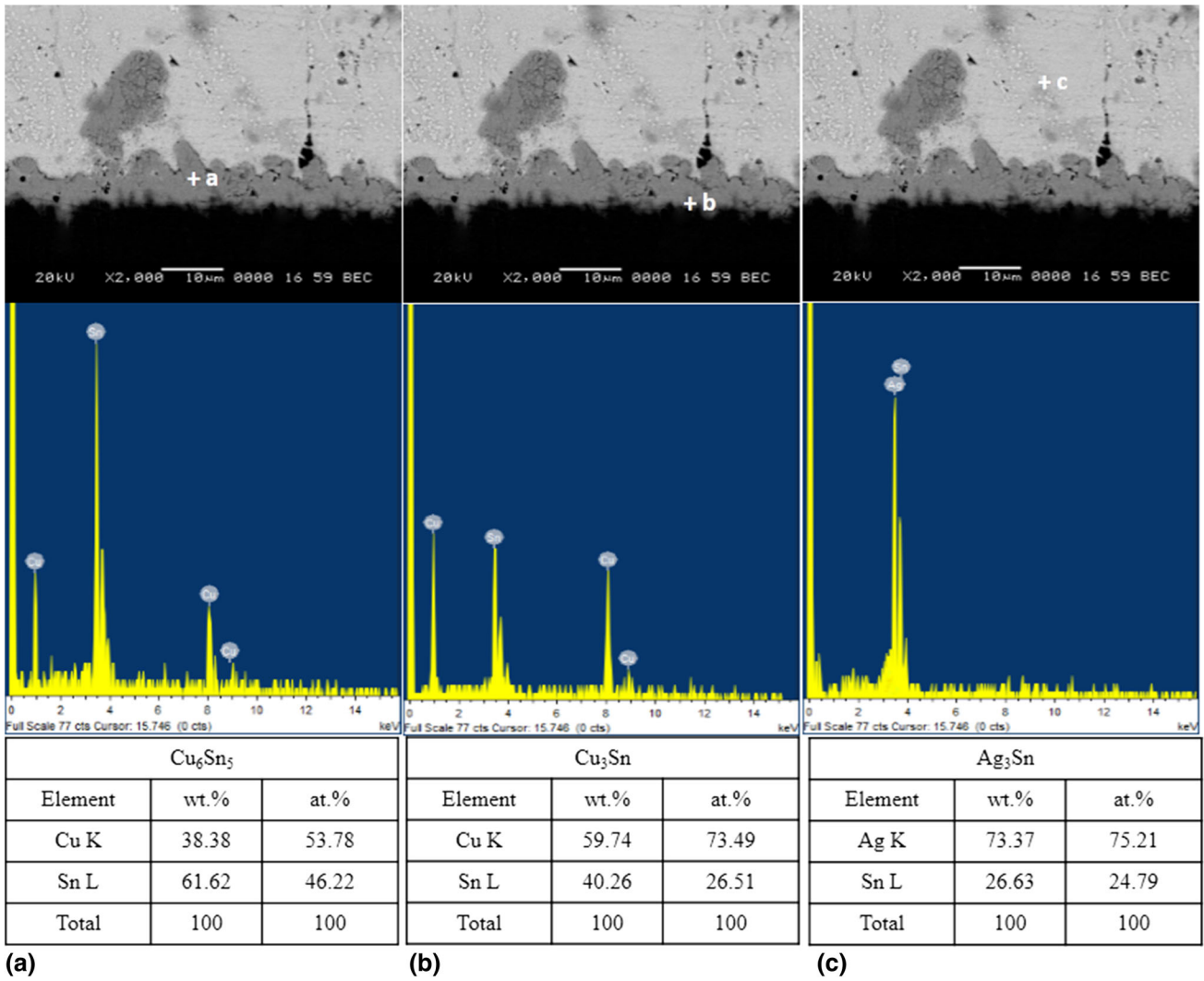


Fig. 9 SEM images and EDS plots showing peaks for different IMCs with the percentage of elemental composition, (a) Cu₆Sn₅, (b) Cu₃Sn, (c) Ag₃Sn

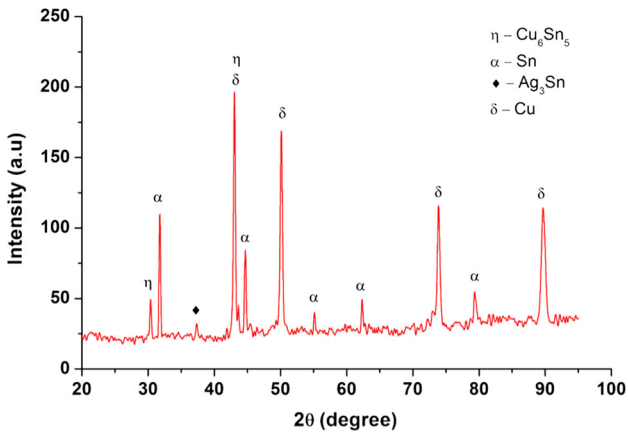


Fig. 10 X-ray diffraction plot of solder/Cu substrate interface for unreinforced SAC305 composition

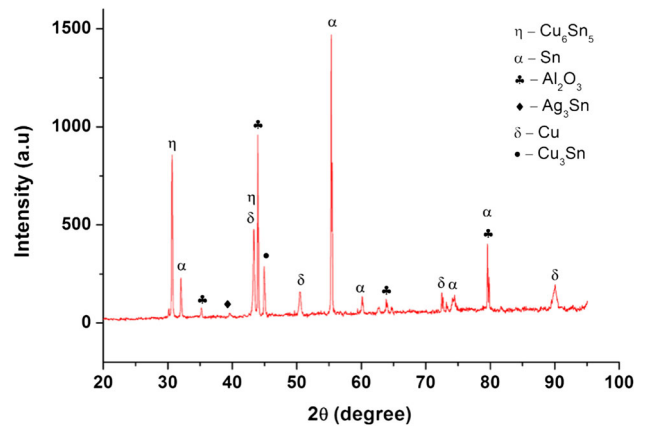


Fig. 11 X-ray diffraction plot of solder/Cu substrate interface for SAC305-0.5Al₂O₃ composition

microstructure. XRD plot for sample reinforced with 0.5 wt.% Al₂O₃ nanoparticles (Fig. 11) confirms the presence of Al₂O₃ nanoparticles at the IMC and solder interfacial region. The

mean IMC thickness as a function of reflow cycle for SAC305 solder with different Al₂O₃ compositions is presented in Fig. 12.

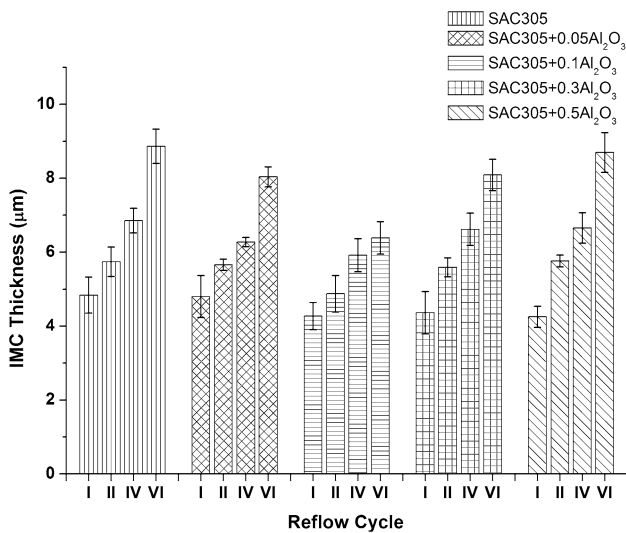


Fig. 12 Effect of reflow cycles on mean IMC thickness

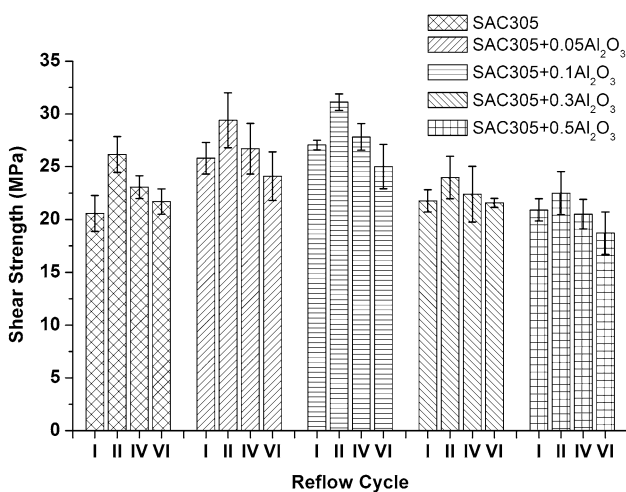


Fig. 13 Joint shear strength of SAC305 solder with different wt.% of Al₂O₃ nanoparticles addition for 1, 2, 4 and 6 reflow cycles

The addition of Al₂O₃ nanoparticles in SAC305 solder suppressed the Cu₆Sn₅ IMC growth under multiple reflow cycles. Ag₃Sn IMCs observed were finer, spheroidal in shape and uniformly dispersed in the Sn matrix. Nanoparticles provide extra nucleation sites which promote high nucleation density of the second phase in the solder matrix. The uniform distribution of second-phase particles like fine spheroidal Ag₃Sn IMCs along with Al₂O₃ nanoparticles improves the solder matrix strength. The suppression of IMC growth can be explained with the help of adsorption theory of surface-active materials (Ref 23). It suggests that the addition of nanoparticles increases the content of the surface-active material in the solder joint which maximizes the amount of adsorbing particles on the IMC surface. An increase in the amount of adsorbing material decreases the surface energy of IMC which results in the decrease in IMC growth rate at the interface as well as in the bulk. In addition, adsorbed Al₂O₃ nanoparticles on Cu₆Sn₅ IMC limits the further dissolution of Cu atoms into liquid solder thus, reducing the grain ripening effect resulting in retardation of IMC growth under multiple reflow cycles

(Ref 15). In the present study, the effectiveness of addition of 0.1 wt.% Al₂O₃ nanoparticles in suppressing the Cu₆Sn₅ IMC growth under multiple reflow cycles was more pronounced than other SAC305-Al₂O₃ compositions. The 0.05 wt.% addition was insufficient to suppress the IMC growth effectively under higher reflow cycles. The higher weight fraction addition above 0.1 wt.% though suppressed the Cu₆Sn₅ IMC growth for single reflow cycle but failed to hinder the growth for higher reflow cycles. The Cu₃Sn IMC formation was not observed for minor Al₂O₃ nanoparticles addition. However, for the addition of 0.3 and 0.5 wt.% Al₂O₃ nanoparticles, a discontinuous Cu₃Sn IMC layer was observed after 4 reflow cycles. This confirms that the addition of Al₂O₃ nanoparticles effectively hinders the dissolution of Cu into the bulk solder and retard the IMC growth under multiple reflow cycles. The reduction of net amount of surface-active nanoparticles due to agglomeration after excessive addition resulted in less adsorption of nanoparticles. This severely reduced all the beneficial effects of Al₂O₃ nanoparticles addition.

3.3 Joint Shear Strength

The shear strength of the solder joint was investigated by the tensile pull test using a micro-lap-shear solder joint on the tensile testing machine. The shear strength of the SAC305 solder alloy with different compositions of Al₂O₃ nanoparticles for 1, 2, 4 and 6 reflow cycles is shown in Fig. 13. The shear strength plot clearly indicates that Al₂O₃ nanoparticles in minor addition (0.05 and 0.1 wt.%) improved the joint shear strength compared to unreinforced as well as SAC305-0.3Al₂O₃ and SAC305-0.5Al₂O₃ compositions under multiple reflow cycles. The shear strength of SAC305 solder alloy (unreinforced and reinforced with nanoparticles) increased up to second reflow and decreased thereafter. The increase in shear strength up to two reflow cycles was due to the formation of thin and uniform Cu₆Sn₅ IMC layer at the joint interface accompanied by uniform dispersion of fine spheroidal Ag₃Sn IMC in bulk microstructure. The uniformly dispersed fine spheroidal-shaped Ag₃Sn IMC strengthen the matrix by dispersion strengthening mechanism during shear failure. Additionally, the dispersed Al₂O₃ nanoparticles in matrix pin the grain boundaries and block the dislocation movement during shear leading to increase in the shear strength.

The shear strength of SAC305 alloy (unreinforced and reinforced with nanoparticles) shows decreasing trend after second reflow cycle. However, the decrease in joint shear strength with higher reflow cycles is less prominent for solder compositions with minor (0.05 and 0.1 wt.%) additions of Al₂O₃ nanoparticles compared to higher (0.3 and 0.5 wt.%) weight fraction addition. The thick Cu₆Sn₅ IMC and the formation of Cu₃Sn IMC cause the mismatch in coefficient of thermal expansion between IMCs leading to the formation of micro-cracks in the IMC layer with multiple reflow cycles. These factors significantly contribute to weakening of the solder joint under stress condition and reduce the joint shear strength.

3.4 Fractography

The fractured surface analysis reveals the failure mode for samples under applied stress and strain conditions. SEM images of fractured samples after shear test for SAC305 solder alloy with Al₂O₃ nanoparticles addition are presented in Fig. 14. The fractured surface investigation revealed that the unreinforced

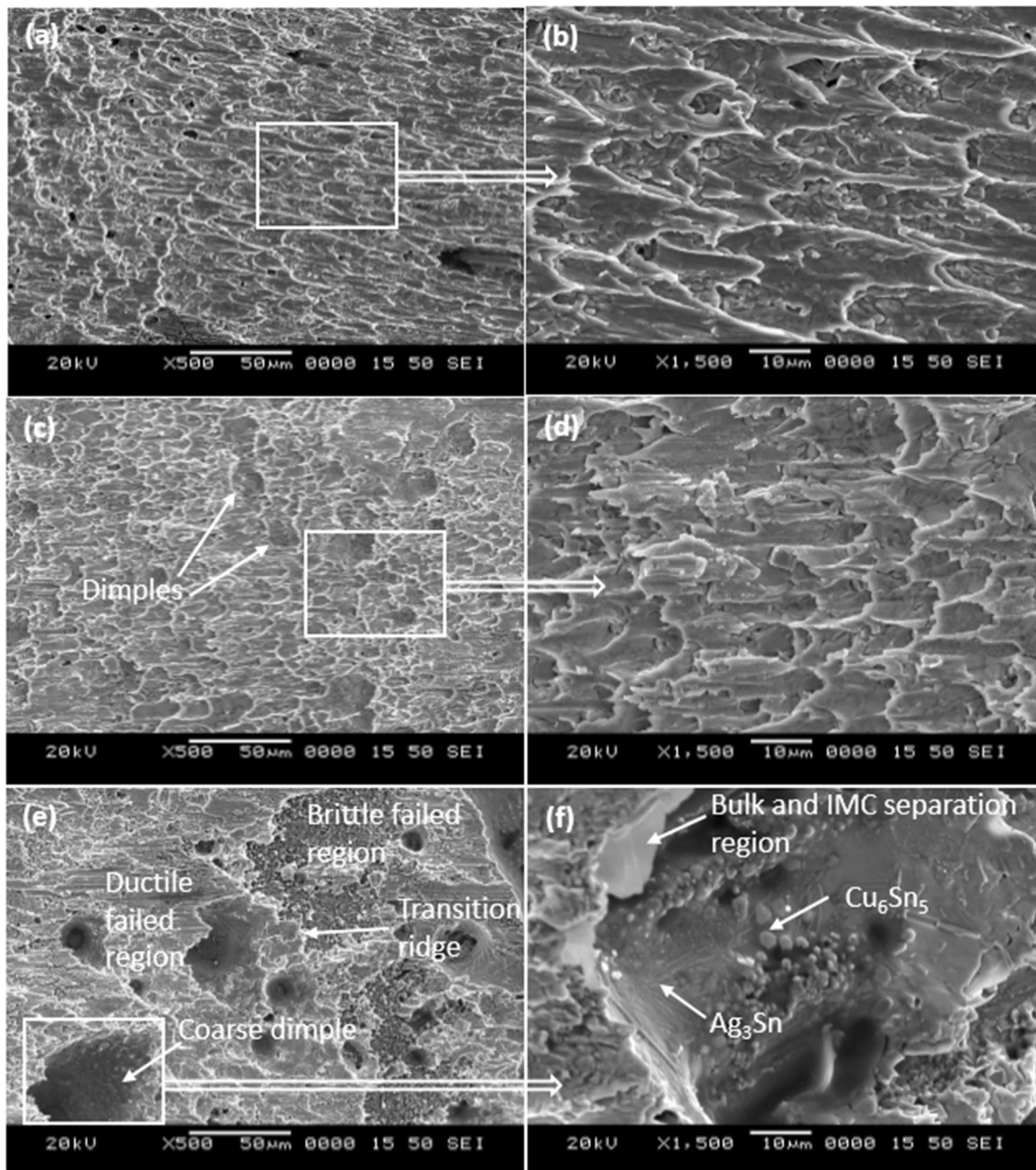


Fig. 14 SEM images of fractured samples after shear test for SAC305 solder alloy with Al_2O_3 nanoparticles addition: (a) fracture surface for unreinforced SAC305 (b) magnified ductile fractured area, (c) ductile fractured surface showing small dimples for SAC305-0.1 Al_2O_3 , (d) enlarged ductile surface with dimples, (e) mixed mode fractured surface showing ductile and brittle fractured region along with transition ridge for SAC305-0.5 Al_2O_3 , (f) magnified coarse dimple area showing broken Cu_6Sn_5 and Ag_3Sn IMCs

SAC305 solder alloy samples reflowed up to 4 reflow cycles failed with ductile fracture, while samples reflowed for 6 reflow cycles failed with mixed mode of failure. Similar failure characteristics were observed for samples of SAC305-0.05 Al_2O_3 , SAC305-0.3 Al_2O_3 and SAC305-0.5 Al_2O_3 solder compositions under similar reflow conditions. The samples added with 0.1 wt.% Al_2O_3 nanoparticles exhibited ductile fracture with small dimples for all the reflow conditions. Figure 14(a) and (b) shows SEM images of a ductile fractured surface for the unreinforced SAC305 solder alloy specimen. Figure 14(c) and (d) shows the ductile failed region with small

dimples of sheared samples for SAC305-0.1 Al_2O_3 composition. The samples fractured with mixed mode failure exhibits the ductile fractured surface with coarse dimples and a brittle failed surface separated with transition ridge. Figure 14(e) shows typical features of mixed mode failure along with fracture transition ridge. The magnified dimple region in Fig. 14(f) shows the shiny broken Cu_6Sn_5 and Ag_3Sn IMCs at the center of the dimple. The fracture appeared to be propagating from bulk solder to the brittle Cu_6Sn_5 IMC at the interface. This is supported by the SEM image (Fig. 14f) showing the solder- Cu_6Sn_5 IMC separation in the fractured

micrograph. The change in fracture behavior from ductile to brittle was attributed to the thicker and coarser scallop Cu₆Sn₅ IMC morphology at the interface.

4. Conclusion

The effects of Al₂O₃ nanoparticles reinforcement on melting behavior, mechanical properties, microstructure evolution at the interface and fracture behavior of SAC305 solder alloy reflowed on Cu substrate for multiple reflow cycles were investigated. The effect on melting temperature (T_L) and melting temperature range of the SAC305 solder alloy with addition of 0.05–0.5 wt.% Al₂O₃ nanoparticles was insignificant. In comparison with monolithic solder alloy, the nanocomposite solders exhibited enhanced solder wettability. The joint shear strength of SAC305 solder alloy increased up to second reflow irrespective of the percentage of nanoparticles addition. The shear strength gradually decreased with higher reflow cycles. In particular, 0.1 wt.% Al₂O₃ nanoparticles addition effectively suppressed the IMC growth, enhanced the joint ductility and consistently improved the joint shear strength of the solder joint under multiple reflow cycles. The addition of over 0.1 wt.% of Al₂O₃ nanoparticles increased the agglomeration and decreased all the beneficial effects of addition of nanoparticles.

References

1. M. Abtey and G. Selvaduray, Lead-Free Solders in Microelectronics, *Mater. Sci. Eng. R Rep.*, 2000, **27**(5), p 95–141
2. L.L. Duan, D.Q. Yu, S.Q. Han, H.T. Ma, and L. Wang, Microstructural Evolution of Sn-9Zn-3Bi Solder/Cu Joint During Long-Term Aging at 170, *J. Alloys Compd.*, 2004, **381**, p 202–207
3. M. Date, T. Shoji, M. Fujiyoshi, K. Sato, and K.N. Tu, Ductile-to-Brittle Transition in Sn-Zn Solder Joints Measured by Impact Test, *Scr. Mater.*, 2004, **51**(7), p 641–645
4. S.P. Yu, M.H. Hon, and M.-C. Wang, The Adhesion Strength of a Lead-Free Solder Hot-Dipped on Copper Substrate, *J. Electron. Mater.*, 2000, **29**(2), p 237–243
5. T. Laurila, V. Vuorinen, and J.K. Kivilahti, Interfacial Reactions Between Lead-Free Solders and Common Base Materials, *Mater. Sci. Eng. R Rep.*, 2005, **49**(1–2), p 1–60
6. G. Kumar and K.N. Prabhu, Review of Non-reactive and Reactive Wetting of Liquids on Surfaces, *Adv. Colloid Interface Sci.*, 2007, **133**(2), p 61–89
7. J. Keller, D. Baither, U. Wilke, and G. Schmitz, Mechanical Properties of Pb-Free SnAg Solder Joints, *Acta Mater.*, 2011, **59**, p 2731–2741
8. A.A. El-Daly and A.M. El-Taher, Evolution of Thermal Property and Creep Resistance of Ni and Zn-Doped Sn-2.0Ag-0.5Cu Lead-Free Solders, *Mater. Des.*, 2013, **51**, p 789–796
9. K. Kanlayasiri, M. Mongkolwongrojn, and T. Ariga, Influence of Indium Addition on Characteristics of Sn-0.3Ag-0.7Cu Solder Alloy, *J. Alloys Compd.*, 2009, **485**(1–2), p 225–230
10. C.L. Chuang, L.C. Tsao, H.K. Lin, and L.P. Feng, Effects of Small Amount of Active Ti Element Additions on Microstructure and property of Sn3.5Ag0.5Cu Solder, *Mater. Sci. Eng. A*, 2012, **558**, p 478–484
11. M.L. Huang and L. Wang, Effects of Cu, Bi, and In on Microstructure and Tensile Properties of Sn-Ag-X(Cu, Bi, In) Solders, *Metall. Mater. Trans. A*, 2005, **36**, p 1439–1446
12. S.M.L. Nai, J. Wei, and M. Gupta, Influence of Ceramic Reinforcements on the Wettability and Mechanical Properties of Novel Lead-Free Solder Composites, *Thin Solid Films*, 2006, **504**(1–2), p 401–404
13. A.K. Gain, Y.C. Chan, and W.K.C. Yung, Effect of Additions of ZrO₂ Nano-Particles on the Microstructure and Shear Strength of Sn-Ag-Cu Solder on Au/Ni Metallized Cu Pads, *Microelectron. Reliab.*, 2011, **51**(12), p 2306–2313
14. M. Amagai, A Study of Nanoparticles in Sn-Ag Based Lead Free Solders, *Microelectron. Reliab.*, 2008, **48**(1), p 1–16
15. T. Fouzder, I. Shafiq, Y.C. Chan, A. Sharif, and W.K.C. Yung, Influence of SrTiO₃ Nano-Particles on the Microstructure and Shear Strength of Sn-Ag-Cu Solder on Au/Ni Metallized Cu Pads, *J. Alloys Compd.*, 2011, **509**(5), p 1885–1892
16. J.S. Lee, K.M. Chu, R. Patzelt, D. Manassis, A. Ostmann, and D.Y. Jeon, Effects of Co Addition in Eutectic Sn-3.5Ag Solder on Shear Strength and Microstructural Development, *Microelectron. Eng.*, 2008, **85**(7), p 1577–1583
17. K. Mohankumar and A.A.O. Tay, Nano-Particle Reinforced Solders for Fine Pitch Applications, 2004, Proceedings of 6th Electronics Packaging Technology Conference (EPTC 2004) (IEEE Cat. No. 04EX971), p 455–461
18. T. Laurila, V. Vuorinen, and M. Paulasto-Kröckel, Impurity and Alloying Effects on Interfacial Reaction Layers in Pb-Free Soldering, *Mater. Sci. Eng. R Rep.*, 2010, **68**(1–2), p 1–38
19. X.L. Zhong and M. Gupta, Development of Lead-Free Sn-0.7Cu/Al₂O₃ Nanocomposite Solders with Superior Strength, *J. Phys. D: Appl. Phys.*, 2018, **41**(9), p 095403
20. T.H. Chuang, M.W. Wu, S.Y. Chang, S.F. Ping, and L.C. Tsao, Strengthening Mechanism of Nano-Al₂O₃ particles reinforced Sn3.5Ag0.5Cu lead-free solder, *J. Mater. Sci. Mater. Electron.*, 2011, **22**(8), p 1021–1027
21. L.C. Tsao, S.Y. Chang, C.I. Lee, W.H. Sun, and C.H. Huang, Effects of Nano-Al₂O₃ Additions on Microstructure Development and Hardness of Sn3.5Ag0.5Cu Solder, *Mater. Des.*, 2010, **31**(10), p 4831–4835
22. Pb-Sn Phase Diagram & Computational Thermodynamics. <https://www.metallurgy.nist.gov/phase/solder/pbsn.html>. Accessed 18 Mar 2018
23. A. Yakymovych, Y. Plevachuk, P. Svec, Sr, P. Svec, D. Janickovic, P. Sebo, N. Beronska, A. Roshanghias, and H. Ipsier, Morphology and Shear Strength of Lead-Free Solder Joints with Sn3.0Ag0.5Cu Solder Paste Reinforced with Ceramic Nanoparticles, *J. Electron. Mater.*, 2016, **45**(12), p 6143–6149